Dalton Transactions

An international journal of inorganic chemistry

Accepted Manuscript

This article can be cited before page numbers have been issued, to do this please use: R. Gericke and J. Wagler, *Dalton Trans.*, 2020, DOI: 10.1039/D0DT01538E.

View Article Online
DOI: 10.1039/D0DT01538E

ARTICLE

(2-Pyridyloxy)arsines as Ligands in Transition Metal Chemistry: A Stepwise As(III)→As(II)→As(I) Reduction

Received 00th January 20xx,
Accepted 00th January 20xx

DOI: 10.1039/x0xx00000x

Robert Gericke*[a] and Jörg Wagler*[a]

Neutral inherently tri- and tetradentate ligands of the type $Ph_{3-x}As(PyO)_x$ (x = 2 (**1**), 3 (**2**)) have been synthesized and characterized. Reaction of **1** with $[RuCl_2(PPh_3)_3]$ affords complex $[PhAs(\mu\text{-}PyO)_2RuCl_2(PPh_3)]$ (**3**), whereas **2** and $[RuCl_2(PPh_3)_3]$ react with formation of $[As(\mu\text{-}PyO)_2RuCl(PPh_3)_2]$ (**5**) and $[Ph_3P(PyO)]Cl$ (**6**). Treatment of complex **5** with [AuCl(tht)] (tht = tetrahydrothiophene) results in liberation of tht and formation of $[AuCl(As(PyO)_2)Ru(PPh_3)_2]$ (**7**), featuring an (Au-As-Ru) core. For compounds **3**, **5**, and **7** the As-Ru and As-Au bond situation has been investigated using NBO, AIM and ELF analysis, allowing the assignment of pronounced canonical forms of σ-(As^{III}→Ru^{II}) to **3**, σ-(As^{II}–Ru^{I}) to **5** and σ-(Au^{I}←As^{I}→Ru^{II}) to **7**.

Introduction

Exploration of synthesis routes toward hetero-bi/trimetallic complexes featuring an E–TM bond or TM–E–TM motif (E: heavier main group metal/metalloid; TM: transition metal) are of current interest in coordination chemistry, with motivation arising from applications of E–TM complexes as anion sensors, their potential general catalytic activity, starting material for chemical vapour deposition or even their capability of small molecule activation.[1] Oxidation states of transition metal bound group 15 elements often range from +III to +V.[2] *N*-Heterocyclic arsenium and stibenium cations as ligands at Pt(0) (**A**, Chart 1)[3] and Co(-1) (**B**)[4] have been investigated. In the resultant hetero-bimetallic complexes a non-coordinating electron pair remains at the pnictogen element.

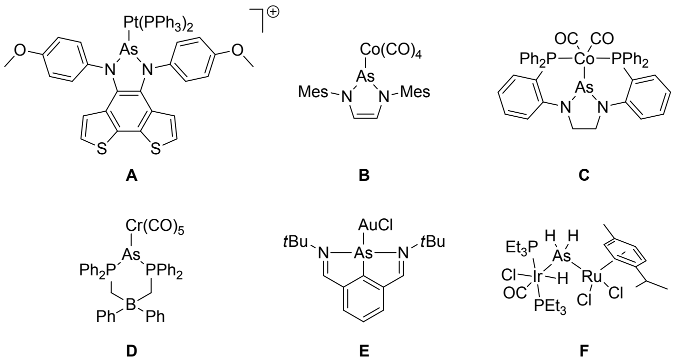

Chart 1. Examples of As-TM-complexes.

Interestingly, Thomas et al. performed NBO (Natural Bond Orbital) analyses on the As-Co-complex **C** (Chart 1), which revealed an almost equal contribution of both atoms to the σ-(As–Co) bond with a slight polarization towards arsenic (As: 54.8%, Co: 45.2%) and a lone pair with high s-contribution at the As center.[5] Ragogna et al. extended their principle of triphosphenium cation[6] towards arsenic in order to stabilize an As(I) species with a bis(phosphine)borate ligand. The resulting compound proved suitable as a σ-donor towards group 6 carbonyls (e.g., compound **D**).[1d] Dostál et al. demonstrated that NCN pincer ligands are capable of stabilizing low-valent As(I) and Sb(I), which were also able to coordinate to late transition metals (Au, Pt) with formation of compounds such as **E**.[7]

To the best of our knowledge, mixed TM hetero-trinuclear complexes featuring arsenic are scarce. Ebsworth et al. presented a synthetic study to form a trimetallic Ir–As–Ru complex (**F**) by oxidative addition of AsH_3 to $[Ir(CO)Cl(PEt_3)_2]$ followed by reaction with $[RuCl_2(cymene)]_2$.[8] Herein we present a route to stepwise forming a trinuclear complex which features a (hitherto unprecedented) Au–As–Ru core. Interestingly, along the synthesis route the As(I) ligand forms from a simple As(III) precursor without the aid of *N*-heterocyclic or bis(phosphine)borate stabilization or NCN-pincer ligands.

Results and discussion

Compounds of type $Ph_{3-x}As(PyO)_x$

Inspired by the syntheses of the phosphorus compounds $PhP(PyO)_2$ and $P(PyO)_3$ (PyO = 2-pyridyloxy),[9] we obtained the corresponding tri- and tetradentate arsenic ligands from reactions of dichlorophenylarsane or arsenic(III) chloride, respectively, with 2-hydroxypyridine (PyOH) in the presence of triethylamine (Et_3N) as supporting base (Scheme 1).

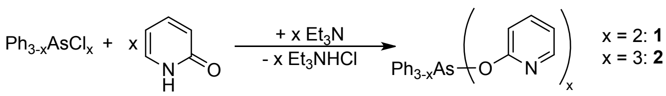

Scheme 1. Synthesis of 2-pyridyloxyarsine ligands **1** and **2**.

[a] Institut für Anorganische Chemie, Technische Universität Bergakademie Freiberg, Leipziger Straße 29, D-09596 Freiberg, Germany.
† Footnotes relating to the title and/or authors should appear here.
Electronic Supplementary Information (ESI) available: [details of any supplementary information available should be included here]. See DOI: 10.1039/x0xx00000x

Both compounds were isolated as colorless and highly hygroscopic solids. Even though elemental analyses confirmed purity of the products, for compound **1** three sets of PyO related ^{1}H NMR signals were observed in an approximate 1:1:1 ratio (Figure 1). The corresponding signals for two different phenyl groups appear in an approximate 1:2 ratio in the ^{1}H NMR spectrum. Hence, there are two different isomers in an approximate 1:2 ratio present in $CDCl_3$ solution, a major isomer with two different As-PyO bonding motifs and a minor isomer with chemically equivalent PyO moieties.

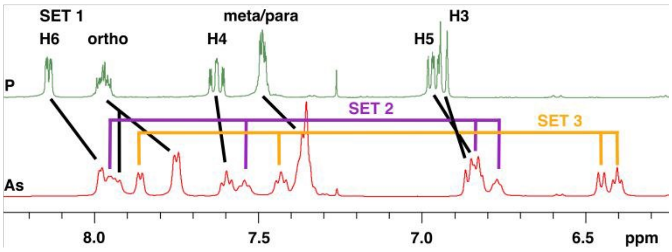

Figure 1. Comparison of the ^{1}H NMR spectra of compound $PhP(PyO)_2$ (top) and $PhAs(PyO)_2$ (**1**, bottom) in $CDCl_3$ solution. Three sets of pyridyloxy related signals in **1** are indicated in black, purple and orange.

According to quantum chemical calculations, out of the symmetric isomers **1^{I}** is thermodynamically more stable than **1^{III}** by approximately 3.31 kcal mol^{-1}, while the isomer **1^{II}** with two different PyO moieties (As-O and As-N bound) is marginally more stable than **1^{I}** (-0.07 kcal mol^{-1}, Chart 2). Therefore, we assign the signals to the isomers **1^{I}** (minor) and **1^{II}** (major component).

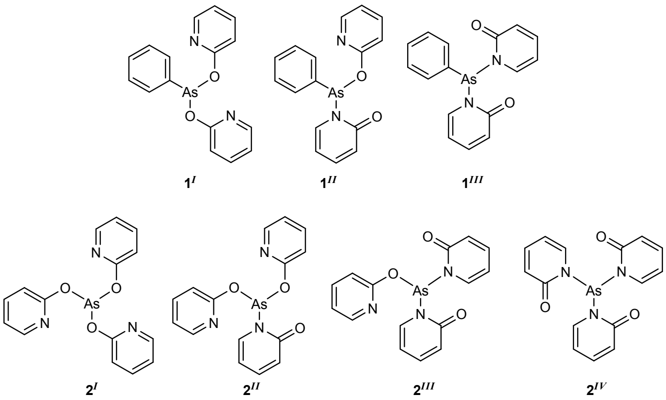

Chart 2. Isomers of compounds **1** and **2**.

The assignment of signals of the minor isomer (set 1) to **1^{I}** is furthermore supported by comparison with spectra of the corresponding phosphorus compound $PhP(PyO)_2$, the ^{1}H and ^{13}C NMR signals of which show only small deviations (merely a slight systematic high field shift of ^{1}H signals of **1^{I}**). Set 2 exhibits the second lowest deviation and can be assigned to the As-O bonded PyO unit in isomer **1^{II}**. Set 3 exhibits the largest deviations and can be assigned to the As-N bonded PyO unit in **1^{II}**.

For compound **2** only one set of broad signals was detected in both the ^{1}H and ^{13}C NMR spectrum. Quantum chemical calculations revealed that there are only small energy differences between the four isomers **2^{I}** (0.44), **2^{II}** (0.00), **2^{III}** (3.56) and **2^{IV}** (3.27 kcal mol^{-1}), whereby isomer **2^{III}** and **2^{IV}** with two or three As–N bonds are the least favored ones. Determination of the molecular structures of compounds **1** and **2** with single-crystal X-ray diffraction (Figure 2) revealed the exclusive presence of the As-O bonding motifs (with weak As···N coordination *trans* to the As-O bonds) for both **1** and **2** in the solid state. The coordination spheres about the arsenic atoms are trigonal pyramidal, with O-As-O angles close to 90° and, in **1**, O-As-C bond angles close to 100°. The molecules exhibit the same conformations as their lighter phosphorus relatives. Compound **1** exhibits a larger deviation between the As1···N1 (2.691(1) Å) and As1···N2 (2.738(2) Å) separation by approximately 0.05 Å, whereas in compound **2** the As···N separations are within a very narrow range (2.68-2.69 Å).

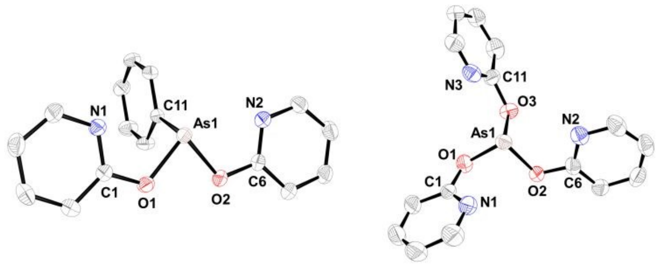

Figure 2. Molecular structures of **1** (left) and **2** (right). Ellipsoids are shown at 50% probability level. Hydrogen atoms have been omitted for clarity. Selected interatomic separations (Å) and angles (deg): **1**: As1-O1 1.843(1), As1-O2 1.839(1), As1-C11 1.943(2), O1-C1 1.349(2), O2-C6 1.348(2), N1-C1 1.324(2), N2-C6 1.323(2), O1-As1-O2 82.78(5), O1-As1-C11 97.26(6), O2-As1-C11 98.60(6), O1-C1-N1 116.24(15), O2-C6-N2 116.99(15); **2**: As1-O1 1.810(3), As1-O2 1.828(3), As1-O3 1.827(3), O1-C1 1.352(6), O2-C6 1.353(6), O3-C11 1.391(8), N1-C1 1.305(6), N2-C6 1.322(5), N3-C11 1.314(5), O1-As1-O2 92.6(1), O1-As1-O3 89.6(2), O2-As1-O3 89.5(2), O1-C1-N1 117.3(4), O2-C6-N2 115.7(4), O3-C11-N3 111.0(8).

In order to shed some light into the discrepancy between the observation of As-N and As-O bonding motifs in solution and only As-O bonding in solid state, relaxed energy surface scans at DFT level of theory were performed. The relaxed energy scans were started from the gas phase optimized structure of isomer **1^{I}** and **1^{II}** (see supporting information for details, Figure S17-S20). The transition state of an isomerization was calculated and compared with its lighter phosphorus analogue where exclusive P-O bonding was observed. The $\Delta G^{\ddagger}$ (Gibbs free energy of the transition state, Figure S21) of an isomerization of **1^{II}** into **1^{I}** was found to be significantly smaller for compound **1** (23.4 kcal mol^{-1}) in comparison to its phosphorus analogues (33.8 kcal mol^{-1}). This trend is in accord with the observation by Garje and Jain, who, for related pentavalent group 15 compounds, reported a tendency for chelate formation at the heavier congener (Sb vs. As).[10] Further analyses (B3LYP cc-pVTZ/SDD(As)-D3(BJ): 16.4 (gas phase), 17.6 kcal mol^{-1} (COSMO($CHCl_3$)); Figure S22) confirmed that the activation barrier could be well below 20 kcal mol^{-1}, thus speaking for possible dynamic isomerization at room temperature.

Reactivity of $Ph_{3-x}As(PyO)_x$ toward $[RuCl_2(PPh_3)_3]$

Reaction of **1** with $[RuCl_2(PPh_3)_3]$ in chloroform results in the formation of the *all-cis* complex $[PhAs(\mu\text{-}PyO)_2RuCl_2(PPh_3)]$ (**3**) with liberation of two equivalents of triphenylphosphine, the release of which was confirmed by ^{31}P NMR spectroscopy (Scheme 2). Ligand **1** coordinates to ruthenium in a *fac* fashion, which leads to a *cis*-coordination of the chlorine atoms. Formation of the related phosphorus complex $[PhP(\mu\text{-}PyO)_2RuCl_2(PPh_3)]$ under similar reaction conditions has been reported.[9] However, compound **1** was observed to appear in two isomers in an approximate ratio of 1:2 for **1′**:**1″**. In order to obtain compound **3** (exclusive As-O bonding mode) in 53% isolated yield, an isomerization of **1″** into **1′** is required (*vide supra*). Reaction of **1** with $[RuCl_2(PPh_3)_3]$ is therefore in accord with a dynamic interconversion of **1″** and **1′**.

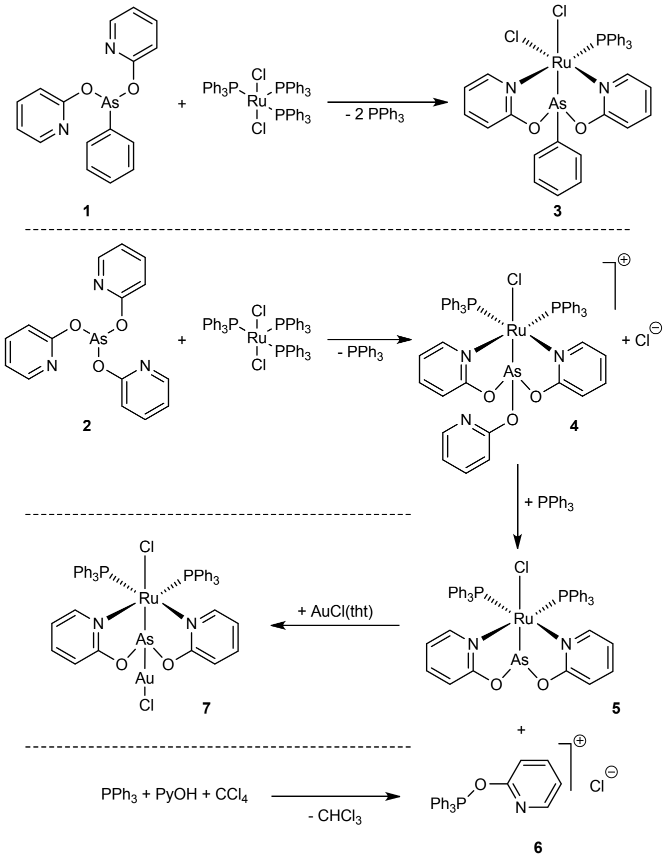

Scheme 2. Syntheses of 2-pyridyloxy-bridged Ru-As complexes.

Further, the reaction of **2** with $[RuCl_2(PPh_3)_3]$ was investigated. In the ^{31}P NMR spectrum of the crude reaction mixture of **2** with $[RuCl_2(PPh_3)_3]$ in $CDCl_3$ after few minutes, one main signal at 34.1 ppm was detected in addition to the signal from free PPh_3 (-5.4 ppm) and signals of much lower intensity at 39.8, 41.8 and 61.6 ppm (Figure S23). We attribute the signal at 34.1 ppm to the arsenic complex $[(\kappa O\text{-PyO})As(\mu\text{-PyO})_2RuCl(PPh_3)_2]Cl$ (**4**). This is supported by the structurally related phosphorus complex $[(\kappa O\text{-PyO})P(\mu\text{-PyO})_2RuCl(PPh_3)_2]PF_6$[9] which exhibits a PPh_3 ^{31}P NMR signal at 36.4 ppm (CD_2Cl_2) whereas neutral complexes of type $[(R)E(\mu\text{-PyO})_2RuCl_2(PPh_3)]$ (E = P, R = Ph, κ*O*-PyO; E = As, R = Ph) exhibit ^{31}P NMR signals for the ruthenium bonded PPh_3 ligand in the range 41.0-41.7 ppm in chloroform solution.[9] Furthermore the ^{13}C NMR signal of the PPh_3 ligands´ *ipso*-carbon atoms exhibits the characteristic multiplet encountered with *cis*-Ph_3P-Ru-PPh_3 arrangements (at 132.6 ppm, Figure S24). Therefore, the smaller signal at 39.8 ppm was assigned to the complex $[(\kappa O\text{-PyO})As(\mu\text{-PyO})_2RuCl_2(PPh_3)]$. Over time, in the ^{31}P NMR spectrum of the crude reaction mixture the intensities of the signals of **4**, uncoordinated PPh_3 and $[(\kappa O\text{-PyO})As(\mu\text{-PyO})_2RuCl_2(PPh_3)]$ decreased, whereby the two signals at 41.8 and 61.6 ppm (reflecting an approximate 2:1 ratio, albeit acquisition parameter settings did not allow for quantitative interpretation) gained intensity. After 7 h, the latter two signals remained in the ^{31}P NMR spectrum, thus indicating compounds **5** and **6** as final products (Scheme 2). Proof of the formation of compound **6** was established by its deliberate synthesis in the reaction of PPh_3 with PyOH and CCl_4 in acetonitrile. As already reported by Appel et al. for similar reactions, $[Ph_3P\text{-}CH_2Cl]Cl$ could be identified as by-product,[11] which could not be separated *via* recrystallization in either CH_2Cl_2/Et_2O or $NCMe/Et_2O$ from **6**. In the ^{31}P and ^{13}C NMR spectra, the chemical shifts for **6** in $CDCl_3$ were identical with those from the crude reaction mixture of **2** with $[RuCl_2(PPh_3)_3]$ after 7 h. We interpret the formation of the neutral complex $[As(\mu\text{-PyO})_2RuCl(PPh_3)_2]$ (**5**) as a reductive elimination of PyO^+ supported by free PPh_3. **5** could be separated from **6** by crystallization (Figure 3). The capability of organophosphanes of performing mild reduction of As(III) compounds has also been reported by Dostál et al..[7a]

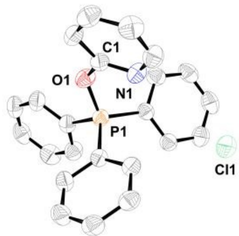

Figure 3. Molecular structure of **6**. Ellipsoids are shown at 50% probability level. Hydrogen atoms have been omitted for clarity. Selected interatomic separations (Å) and angles (deg): P1-C6 1.786(4), P1-C12 1.792(4), P1-C18 1.783(3), P1-O1 1.587(3), O1-C1 1.408(5), N1-C1 1.309(5), C6-P1-C12 110.8(2), C6-P1-C18 112.1(2), C12-P1-C18 110.0(2), P1-O1-C1 122.2(2), O1-C1-N1 116.1(3).

Table 1. Selected bond lengths (Å) and angles (°) of **3**, **5** and **7**. For the second molecule in the asymmetric unit of **5**·$2CHCl_3$ corresponding bond lengths and angles are reported after the slash.

	3	5	7
As1-Ru1	2.2386(4)	2.3124(3) / 2.3019(3)	2.2919(5)
As1-Au1			2.3283(6)
Ru1-N1	2.112(3)	2.139(2) / 2.174(2)	2.172(3)
Ru1-N2	2.182(3)	2.184(2) / 2.137(2)	2.168(3)
Ru1-P1	2.299(1)	2.339(1) / 2.359(1)	2.391(1)
Ru1-P2		2.353(1) / 2.336(1)	2.385(1)
Ru1-Cl1	2.414(1)	2.547(1) / 2.539(1)	2.459(1)
Ru1/Au1-Cl2	2.421(1)		2.288(1)
As1-O1	1.811(2)	1.906(2) / 1.914(2)	1.869(3)
As1-O2	1.821(2)	1.889(2) / 1.896(2)	1.852(3)
As1-C1/Au1	1.905(3)		2.3284(4)
N1-Ru1-N2	86.10(10)	82.81(7) / 79.65(3)	79.79(12)
N1-Ru1-P2/Cl1	172.23(7)	173.15(5) / 167.74(5)	168.35(9)
N2-Ru1-P1	179.06(8)	167.15(5) / 169.15(5)	168.35(9)
P1-Ru1-P2/Cl1	89.31(3)		103.97(3)
As1-Ru1-Cl1	93.17(2)	168.96(2) / 168.86(1)	170.70(3)
As1-Ru1-Cl2	169.85(2)		
O1-As1-O2	99.37(12)	92.64(8) / 91.34(7)	92.23(15)
Ru1-As1-C11/Au1	149.43(10)		144.98(2)
As1-Au1-Cl2			176.67(3)

View Article Online
DOI: 10.1039/D0DT01538E

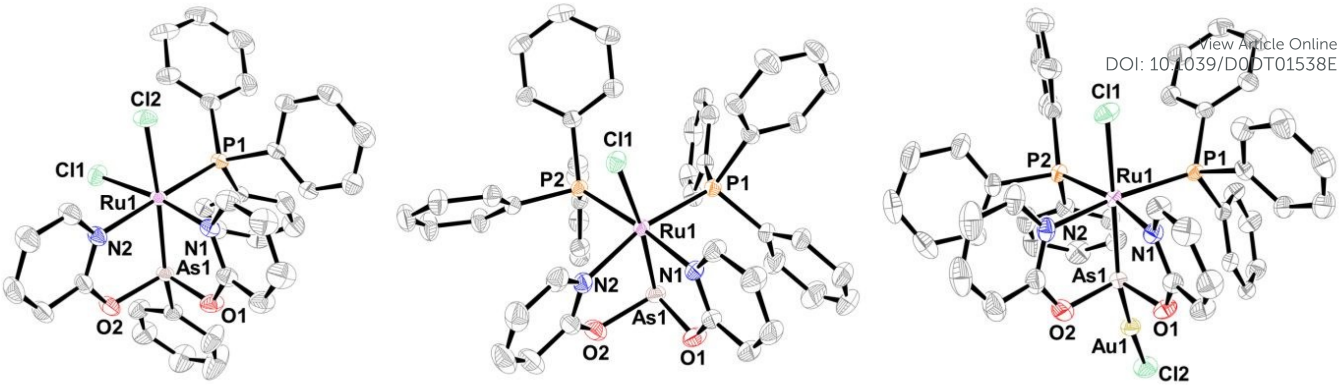

Figure 4. Molecular structures of **3**·1.5CHCl$_3$ (left), **5**·2CHCl$_3$ (middle) and **7**·CHCl$_3$ (right). Ellipsoids are shown at 50% probability level. Hydrogen atoms and solvent molecules have been omitted for clarity. For compound **5** only one of the two independent (but conformationally similar) molecules in the asymmetric unit is shown as a representative example.

For compounds **3** and **5** we succeeded in growing crystals suitable for single-crystal X-ray diffraction analyses (Figure 4, Table 1). In **3** the ruthenium atom is distorted octahedral coordinated in an *all-cis* configuration, and its molecular structure in **3**·1.5CHCl$_3$ reveals the expected analogies with the related phosphorus complex [PhP(μ-PyO)$_2$RuCl$_2$(PPh$_3$)] (for molecular overlay see Figure S25). Notably, the Ru1–As1 bond is significantly shorter than the shortest Ru–As bonds reported so far (2.31 Å) by Powell et al..[12,13] Nonetheless, the Ru1–As1 bond is significantly longer than the corresponding Ru–P bond in the related complex [PhP(μ-PyO)$_2$RuCl$_2$(PPh$_3$)] (by about 0.1 Å), as expected for a larger donor atom. Also, its As lone pair donor capability seems to be weaker with respect to the related phosphorus complex, which is reflected by significant shortening of the *trans*-disposed Ru1–Cl2 bond by about 0.04 Å. The rather wide Ru1-As1-C11 angle (149.4(1)°) allows to interpret the As coordination sphere ($\tau_4{}'$ = 0.62)[14] as intermediate between seesaw ($\tau_4{}' \leq 0.36$, with $\alpha \geq 90°$) and tetrahedral ($\tau_4{}'$ = 1).

In complex **5** the ruthenium coordination sphere is distorted octahedral. The angles around As1 are smaller than 97°, whereby the As coordination sphere is best described as trigonal pyramidal. In spite of the lower As coordination number, the average Ru-As bond length is approximately 0.07 Å longer than in complex **3**. (Also, the Ru-P bonds are in average elongated by approximately 0.05 Å). Interestingly, with respect to complex **3** even the As–O bonds are elongated by approximately 0.07-0.10 Å in spite of the lower coordination number of As1 in **5**. This feature can be attributed to a higher electron density around As1 in **5** than in **3** (i.e., lower oxidation state and larger covalent radius), which is in accord with the lower natural charge at As (**3**: NC$_{As}$ = 1.70 e, **5**: NC$_{As}$ = 0.99 e). Furthermore, in combination with the longer As–O bonds the average O–C bond lengths are significantly shorter in **5** than in **3** (by approximately 0.021(7) Å), thus indicating a transition from the As–O–C=N mode in **3** to the As←O=C–N mode in **5**.

Reactivity of 5 toward [AuCl(tht)]

As the arsenic atom in **5** exhibits a lone-pair, we were interested in its ligand qualities. In spite of the bulky PPh$_3$ ligands, a soft linear coordinating metal (like gold(I)) should be able to utilize this Lewis basic site. Treating a chloroform solution of **5** with [AuCl(tht)] (tht = tetrahydrothiophene) leads to a high field shift of the ^{31}P NMR signal by about 4 ppm and retention of the characteristic multiplet in the ^{13}C NMR spectrum for the *ipso*-carbon, which is shifted from 135.9 (**5**) to 133.9 ppm (**7**), thus indicating that the *cis*-Ru(PPh$_3$)$_2$ motif remains intact. Upon vapour diffusion of *n*-pentane into a CHCl$_3$ solution of **7**, crystals suitable for single-crystal X-ray diffraction have formed. The molecular structure of the expected complex [AuCl(As(μ-PyO)$_2$)RuCl(PPh$_3$)$_2$] (**7**), featuring a hitherto unprecedented Au-As-Ru core, is shown in figure 4 (right). The Ru–P bonds in **7** are elongated (on average) by approximately 0.04 Å with respect to compound **5**. The As→Au coordination results in a shortening of the Ru1–Cl1 bond by approximately 0.08 Å (relative to **5**). With the wide Au1-As1-Ru1 angle of 144.98(2)° the As1 coordination sphere can again be described as intermediate between seesaw and tetrahedral ($\tau_4{}'$ = 0.66).[14] This coordination sphere is different from the one of another literature reported complex with Au-*Pn*-Ru motif (*Pn* = pnictogen): Bedford et al. reported a heterodinuclear phosphaalkenyl complex, which has an Au-P-Ru angle of 120.1(1)° due to the trigonal-planar coordination sphere around the phosphaalkenyl ligand.[15]

Natural Bond Orbital Analysis

In order to assign formal oxidation states and to investigate the bond characteristics of compounds **3**, **5** and **7**, we performed quantum chemical calculations. The natural localized molecular orbital (NLMO) representative of the As–Ru σ-bond exhibits predominant As contribution in **3** (Table 2, Figure S26). The high

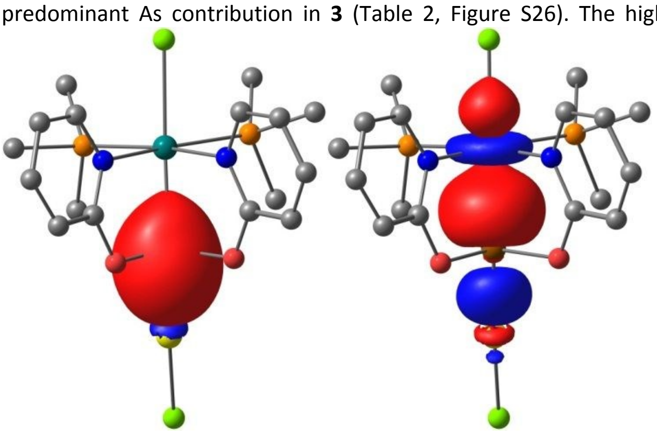

Figure 5. NLMO representations of σ-(As→Au) bond (left) and σ-(As→Ru) bond (right) in **7** are shown at an isosurface value of 0.06. Only the *ipso*-carbon atoms of the PPh$_3$ ligands are depicted, and H-atoms are omitted for clarity.

View Article Online
DOI: 10.1039/D0DT01538E

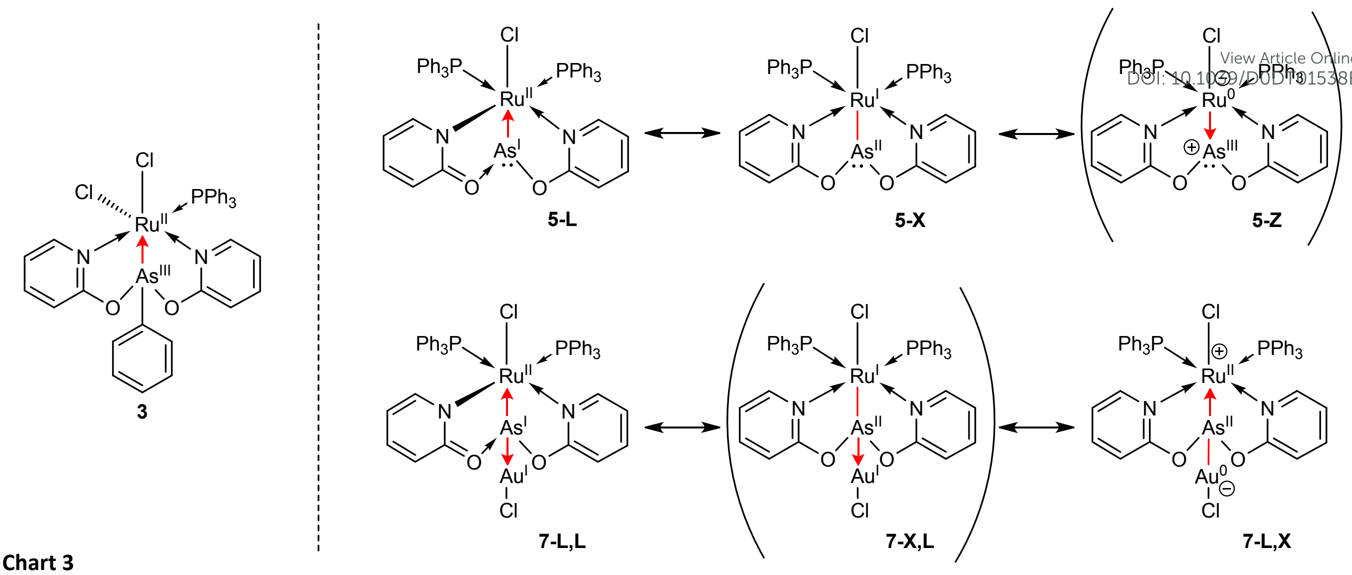

Chart 3

4s-population from the As atom in that bond, and the high natural charge (NC) of the As atom, speak for an $As^{III}\rightarrow Ru^{II}$ canonical form, where the electron pair at arsenic acts as donor towards ruthenium (Chart 3). In comparison to **3**, the NCs of As and Ru in **5** dropped by 0.71 and 0.17 e, respectively. At the arsenic atom a lone pair with predominant 4s character (78.1%, Figure S27) was found by NLMO analysis. The σ-(As–Ru) bond exhibits almost equal arsenic (51%) and ruthenium (44%) contributions. To assign formal oxidation states to the $(As/Ru)^{III}$ core in **5**, the L/X/Z-formalism from Green was considered.[16] The reduction of the natural charges for both atoms and their similar NLMO contributions are in support of the X-type description with (As^{II}–Ru^{I}) core (**5-X**) as the formal As–Ru-bond situation in **5**. The slight polarization towards As and the uneven reduction of the natural charges, however, speak for a slight L-type contribution in terms of an ($As^{I}\rightarrow Ru^{II}$) core (**5-L**). The latter contribution to the As–Ru σ-bond clearly increases in **7**, reflected by the higher NC at Ru and less Ru contribution in the σ-As–Ru NLMO (Figure 5).

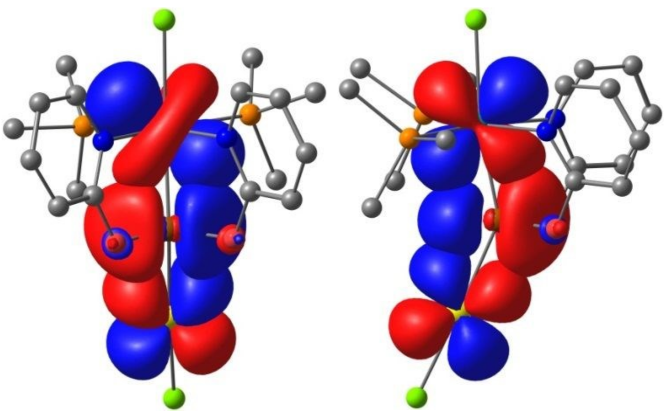

Figure 6. NBO representations of π-(Au→As←Ru) backbonding in **7** are shown at an isosurface value of 0.06. Only the *ipso*-carbon atoms of the PPh_3 ligands are depicted, and H-atoms are omitted for clarity.

The σ-(As–Au) bond clearly can be described as a donor-acceptor interaction of the 4s-lone pair of As donating into the 6s-orbital of Au. These results of NLMO analysis support assignment of the formal oxidation states of an ($Au^{I}\leftarrow As^{I}\rightarrow Ru^{II}$) core. The lower NC at Ru^{II} in comparison to Au^{I} can be attributed to the better charge compensation by six ligands at ruthenium versus two ligands at gold. For complexes **3**, **5** and **7**, π-(As←Ru) backbonding was found from the ruthenium $4d_{xz}$ and $4d_{yz}$ orbitals into the two vacant As 4p orbitals. Additionally, π-(As←Au) backbonding from the gold atom´s $5d_{xz}$ and $5d_{yz}$ was observed in complex **7** (Figure 6).

Table 2. Natural charges (NC in e) and NLMO characteristics of **3**, **5** and **7**.

	3	5	7
NC(Ru)	−0.02	−0.19	−0.13
NC(Au)			0.33
NC(As)	1.70	0.99	1.06
NLMO: σ-(As-Ru)	29.1% Ru 68.0% As As (64.2% 4s, 35.7% 4p)	44.8% Ru 51.2% As As (14.3% 4s, 85.3% 4p)	33.6% Ru 5.7% Au 56.3% As As (10.1% 4s, 89.7% 4p)
Percentage of parent NBO	94.1%	93.1%	86.3%
NLMO: σ-(As-Au)			2.2% Ru 10.2% Au 83.4% As As (82.3% 4s, 17.5% 4p)
Percentage of parent NBO			82.3%

NBO analysis aims at finding the optimal Lewis structure even though multiple resonance forms are feasible. If deviation from this localized form is present (e.g., in phenyl rings), an indication of delocalization is given by a drop in NBO occupancy (percentage of parent NBO in NLMO, the latter of which is set to accommodate two electrons). In aromatic systems like phenyl rings this depletion is approximately from ≈98% to ≈83%. A related loss of two-atomic NBO contributions in the NLMOs is observed along the trimetallic Au-As-Ru core. In this particular case, another indication of delocalization is reflected by the noticeable Au contribution (5.7%) in the σ-(As-Ru) NLMO.

Quantum Theory of Atoms in Molecules

The topological analysis (atoms in molecules, AIM[17]) of complexes **3**, **5** and **7** were conducted to shed light into the delocalization effects observed in NLMO analysis. As the latter did not allow for a direct comparison of highly localized two-center bonds, we inspected the features of the individual bond critical points (BCPs, Table 3). BCPs along the As–Ru bond paths confirmed the presence of As–Ru bonds in **3**, **5** and **7**. The electron density ($\rho(\mathbf{r_b})$) varies within a narrow range (0.749-0.780 e·Å^{-3}). Some topological parameters at the BCP can be used to classify bond types. The ratio $|V(\mathbf{r_b})|$ / $G(\mathbf{r_b})$ (with $V(\mathbf{r_b})$ = potential energy density, $G(\mathbf{r_b})$ = Lagrangian kinetic energy) at the BCPs lays in the range $1 < |V(\mathbf{r_b})| / G(\mathbf{r_b}) < 2$[18] and is thus indicative for an intermediate bond characteristic (covalent bond with additional ionic contribution; $1 > |V(\mathbf{r_b})| / G(\mathbf{r_b})$: pronounced ionic character; $|V(\mathbf{r_b})| / G(\mathbf{r_b}) > 2$: covalent interaction). The NCs (As: 1.06–1.70; Ru: −0.02 to −0.13 e) are in support of attractive noncovalent bond contributions. The magnitude of the ratio $|V(\mathbf{r_b})| / G(\mathbf{r_b})$ (increase of covalent characteristics) follows the order **3** < **7** < **5**. According to Macchi et al., the Laplacian of electron density ($\nabla^2\rho(\mathbf{r_b})$) is a good indicator for the bond properties. For complex $[Co_2(CO)_6(AsPh_3)_2]$, the authors reported $\nabla^2\rho(\mathbf{r_b})$ of 1.344(8) e·Å^{-5} for the Co–Co bond as well as 4.25(2) e·Å^{-5} and 4.21(2) e·Å^{-5} for the As→Co bonds.[19] Whereas this characteristic of the As–Ru bond in **5** is similar to the former (thus being closer to a nonpolar bond), the Laplacian of the As–Ru bond in **3** is closer to the latter, while the characteristics (also for the As–Au bond) in **7** are intermediate. Also, the ratio $G(\mathbf{r_b})/\rho(\mathbf{r_b})$ provides information about the difference between shared interactions (<1) and donor-acceptor interactions (≈1).[19] The ratio $G(\mathbf{r_b})/\rho(\mathbf{r_b})$ is in general <1 and its magnitude decreases in the order **3** < **7** < **5**. The conclusion from the trend of the Laplacian of the As-TM bonds are in agreement with the trends found in the $G(\mathbf{r_b})/\rho(\mathbf{r_b})$ ratio. According to the group of topological parameters of the As→Ru bonds described above, the bond characteristics are ranging between closed shell donor-acceptor interaction ($\rho(\mathbf{r_b})$ = small; $G(\mathbf{r_b})/\rho(\mathbf{r_b}) \approx 1$; $H(\mathbf{r_b}) < 0$; $\nabla^2\rho(\mathbf{r_b}) > 0$; $1 < |V(\mathbf{r_b})| / G(\mathbf{r_b}) < 2$) for compounds **3** and **7** and metallic shared interaction ($\rho(\mathbf{r_b})$ = small; $G(\mathbf{r_b})/\rho(\mathbf{r_b}) < 1$; $H(\mathbf{r_b}) < 0$; $\nabla^2\rho(\mathbf{r_b}) \approx 0$; $1 < |V(\mathbf{r_b})| / G(\mathbf{r_b}) < 2$) for compound **5**. The depletion of ELF (electron localization function)[20] between the As and Ru atoms in **3** and **7** supports the pronounced donor-acceptor interaction in those complexes in comparison to the As–Ru bond in **5** (Figure 7).

Noteworthy, the AIM properties at the BCP of the As–Au bond in **7** are intermediate between those found for the As–Ru bonds in **5** and **7**. Also the ELF map exhibits a rather weak depletion between gold and arsenic, which would hint at As–Au bond properties closer to pronounced metallic shared type rather than donor-acceptor interaction. This observation stands in contrast to the strong polarization of the σ-(As→Au) bond found by NBO analysis. However, delocalization of Au contributions across the Au-As-Ru core (into the σ-As–Ru NLMO) is in agreement with the properties at the Au–As BCP.

Table 3. Selected features of the bond critical points (BCPs) of the As–TM bonds in compounds **3**, **5**, and **7** derived from the topological analyses (AIM).

Feature [a]	**3** $_{As-Ru}$	**5** $_{As-Ru}$	**7** $_{As-Ru}$	**7** $_{As-Au}$
$\rho(\mathbf{r_b})$	0.767	0.780	0.749	0.760
$\nabla^2\rho(\mathbf{r_b})$	3.960	1.310	2.753	1.864
$G(\mathbf{r_b})$	0.658	0.482	0.550	0.513
$V(\mathbf{r_b})$	−1.039	−0.873	−0.908	−0.895
$\|V(\mathbf{r_b})\|/G(\mathbf{r_b})$	1.579	1.810	1.650	1.745
$G(\mathbf{r_b})/\rho(\mathbf{r_b})$	0.859	0.619	0.735	0.674
$H(\mathbf{r_b})$	−0.381	−0.390	−0.357	−0.382
$H(\mathbf{r_b})/\rho(\mathbf{r_b})$	−0.497	−0.501	−0.478	−0.503
Ellipticity	0.238	0.063	0.094	0.007

[a] Electron density ($\rho(\mathbf{r_b})$ in e·Å^{-3}), Laplacian of electron density ($\nabla^2\rho(\mathbf{r_b})$ in e·Å^{-5}), Lagrangian kinetic energy density ($G(\mathbf{r_b})$ in Hartree·Å^{-3}), potential energy density ($V(\mathbf{r_b})$ in Hartree·Å^{-3}), ratio $|V(\mathbf{r_b})|/G(\mathbf{r_b})$, ratio $G(\mathbf{r_b})/\rho(\mathbf{r_b})$ in Hartree·e^{-1}, electron energy density ($H(\mathbf{r_b})$ in Hartree·Å^{-3}), ratio $H(\mathbf{r_b})/\rho(\mathbf{r_b})$ in Hartree·e^{-1}.

Conclusions

Herein, the 2-pyridyloxy functionalized arsine ligands $PhAs(PyO)_2$ (**1**) and $As(PyO)_3$ (**2**) have been synthesized and characterized. In solution they exhibit dynamic isomerization through exchange between As–O and As–N bonding modes. Starting from $As(PyO)_3$, we demonstrated a new synthesis method to access low valent arsenic complexes *via* reductive elimination of the auxiliary PyO ligand supported by PPh_3 with formation of $[(PyO)PPh_3]^+Cl^-$ (**6**). The complex $[As(\mu\text{-}PyO)_2RuCl(PPh_3)_2]$ (**5**) is the product of this two electron reduction and exhibits a σ-(As^{II}–Ru^{I}) core as dominant canonical form in addition to contributions of σ-(As^{I}→Ru^{II}) donor-acceptor characteristics. This is in contrast to the formation of metallaboratranes, where reductive elimination (of a hydrocarbon R-H) from a H-$B^{III}Ru^{II}$-R core results in predominant reduction of Ru with formation of a B^{III}←Ru^{0} dative bond.[21] Addition of an AuCl source leads to the formation of complex $[AuCl(As(\mu\text{-}PyO)_2)RuCl(PPh_3)_2]$ (**7**), featuring an Au-As-Ru core. According to NBO and AIM calculations contributions of both canonical forms σ-(Au^{I}←As^{I}→Ru^{II}) and σ-(Au^{0}–As^{II}→Ru^{II}) should be taken into consideration for this trinuclear bonding situation. Due to the coordination of the AuCl moiety to **5** an electron density shift

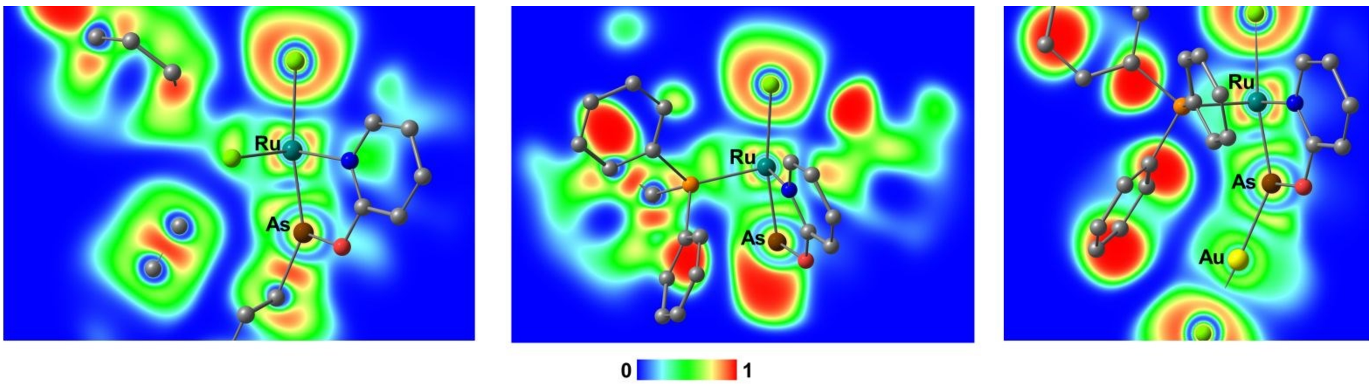

Figure 7. Electron Localization Function (ELF) of **3** (left), **5** (middle) and **7** (right).

in the As–Ru bond results, which leads to a change of the formal X-type As^{II}–Ru^{I} bond to an L-type As^{I}→Ru^{II} bonding mode and therefore formal reduction of the arsenic atom caused by coordination of an additional metal atom.

Experimental

General considerations

All preparations were carried out under an atmosphere of dry argon using standard Schlenk techniques. $[RuCl_2(PPh_3)_3]$ was synthesized following a literature protocol starting from elemental ruthenium.[22] [AuCl(tht)] was synthesized along a literature method starting from elemental gold.[23] $PhP(PyO)_2$ was synthesized following the literature method.[9] Tetrahydrofuran (THF) and triethylamine (Et_3N) were distilled from sodium/benzophenone and stored under dry argon. Dichloromethane (DCM) was distilled from calcium hydride and stored under argon. Chloroform (stabilized with amylenes), n-pentane and acetonitrile were stored over molecular sieves 3 Å. All other chemicals used were commercially available and were used without further purification.

Caution: Arsenic compounds such as $AsCl_3$, $PhAsCl_2$ and derivatives thereof are highly toxic and, in case of $AsCl_3$ and $PhAsCl_2$, volatile. Safety precautions need to be obeyed!

Materials and Equipment

Elemental analyses (C, H, N) were performed on a 'Vario Micro Cube' analyzer (Elementar, Hanau, Germany).

Solution NMR spectra were recorded on an "Avance III 500" or "Ascend NanoBay 400" spectrometer (Bruker Biospin, Rheinstetten, Germany) and internally referenced to tetramethylsilane for ^{1}H and ^{13}C and externally referenced to 85% H_3PO_4 for ^{31}P. The $^{31}P\{^{1}H\}$ NMR spectra at "Avance III 500" were recorded as 1D sequence with inverse gated decoupling using 30° flip angle and D1 = 5 s; at "Ascend NanoBay 400" they were recorded as 1D sequence with pulsed gated decoupling using 30° flip angle and D1 = 2 s. 90° ^{1}H BB-decoupling was used. Signals were assigned by using $^{1}H,^{1}H$-COSY, $^{1}H,^{13}C$-HSQC, $^{1}H,^{13}C$-HMBC and $^{1}H,^{1}H$-NOESY techniques.

Single-crystal X-ray diffraction data sets were collected with ω-scans on an 'IPDS-2(T)' diffractometer (STOE, Darmstadt, Germany) using Mo-K_{α}-radiation. Absorption correction was performed with XShape using integration correction type. Structures were solved by direct methods with ShelXS[24] and all non-hydrogen atoms were anisotropically refined in full-matrix least-squares cycles against $|F^2|$ (ShelXL).[25] Hydrogen atoms were placed in idealized positions and refined isotropically (riding model). Selected parameters of data collection are listed in tables S1 and S2. CIF files have been deposited with the Cambridge Crystallographic Data Center (CCDC) and can be obtained free of charge (for inquiry contact: CCDC, 12 Union Road, Cambridge, CB2 1EZ, UK, fax: +44−1223−336033, e-mail: deposit@ccdc.cam.ac.uk) quoting the following reference numbers: CCDC-1994837 (**6**), 1994838 (**2**), 1994839 (**3**·1.5$CHCl_3$), 1994840 (**1**), 1994841 (**7**·$CHCl_3$), 1994842 (**5**·2$CHCl_3$).

Computational analyses of **1**, **2** and $PhP(PyO)_2$ were carried out with ORCA 4.1.2[25] using DFT-PBEPBE functional using cc-pVTZ[27] basis set for all atoms and effective core potential for As [SD(28,MWB)][28] and D3BJ[29] dispersion correction during geometry optimization (atomic coordinates are given in the supporting information). Further information of the optimization of the transition state of the isomerization of **1**$''$ into **1**$'$ is given in the supporting information. Optimization of the H-atom positions for complexes **3**, **5**, and **7** were carried out with ORCA 4.1.2[26] using DFT-PBEPBE functional, def2-TZVPP[30] basis set for all atoms and effective core potentials for Ru [SD(28,MWB)] and Au [SD(60,MWB)].[28] Starting from those structures, NBO (Natural Bond Orbital) and NLMO (Natural Localized Bond Orbital) calculations have been performed using ORCA 4.1.2[26] with the NBO 6.0 package[31] using DFT-B3LYP functional (VWN-3) and for M = As, Ru: old-DKH-TZVPP, M = Au: SARC-DKH-TZVPP and C, H, N, O, P, Cl: DKH-def2-TZVPP basis set including Douglas-Kroll-Hess 2nd order scalar relativistic. NBO graphics were generated using ChemCraft.[32] Topological analyses were performed with MultiWFN.[33]

Synthesis of $PhAs(PyO)_2$ (1)

$PhAsCl_2$ used as starting material was synthesized along a slightly modified method according to Michaelis et al.[34] starting from PhAsO. PhAsO (2.00 g, 11.9 mmol) and conc. HCl (60 mL) were stirred at 60 °C for 20 min. The aqueous phase was extracted with CH_2Cl_2 (3 × 5 mL). The combined organic phases were evaporated to dryness (condensation of volatiles into a cold trap under reduced pressure) and the residue was distilled at 120 °C/10 Torr (Yield: 1.70 g, 7.63 mmol, 64%).

In a Schlenk flask, 2-hydroxypyridine (500 mg, 5.26 mmol) and triethylamine (638 mg, 6.30 mmol) were dissolved in THF (10 mL). $PhAsCl_2$ (586 mg, 2.63 mmol) was added dropwise, and the resultant white suspension was stirred at ambient temperature for 3 h, whereupon the white precipitate of Et_3NHCl was filtered and washed with THF (3 mL). The combined filtrate and washings were evaporated to dryness (condensation of volatiles into a cold trap under reduced pressure), and the residue was recrystallized from THF (1.5 mL). The white crystalline solid obtained after storing at 4 °C for one week was suitable for single-crystal X-ray diffraction. The supernatant was decanted, the white solid was washed with Et_2O (3 mL) and dried *in vacuo*. The compound is highly hygroscopic. Yield: 346 mg (1.01 mmol, 38%), in solution this compound co-exists in two isomers;

^{1}H NMR (500.1 MHz, $CDCl_3$): 6.40 (m, PyO-**1**$''$, 2H), 6.45 (m, PyO-**1**$''$, 2H), 6.77 (m, PyO-**1**$''$, 2H), 6.78-6.88 (m, PyO-**1**$'$/**1**$''$, 6H), 7.31-7.39 (m, *meta*/*para*-Ph-**1**$''$/**1**$'$, 9H), 7.43 (m, PyO-**1**$''$, 2H), 7.54 (m, PyO-**1**$''$, 2H), 7.59 (m, PyO-**1**$'$, 2H), 7.75 (m, *ortho*-Ph-**1**$''$, 6H), 7.86 (m, PyO-**1**$''$, 2H), 7.89-8.01 (br. m, *ortho*-Ph-**1**$'$, PyO-**1**$''$/**1**$'$, 6H); $^{13}C\{^{1}H\}$ NMR (125.8 MHz, $CDCl_3$): 108.3 (PyO-**1**$''$), 111.2 (PyO-**1**$'$), 116.2 (PyO-**1**$''$), 116.8 (PyO-**1**$'$), 117.8 (PyO-**1**$''$), 128.3 (Ph), 128.5 (Ph), 130.3 (2xPh), 130.4 (2x PyO-**1**$''$, 2xPh), 137.3 (PyO-**1**$''$), 139.2 (PyO-**1**$''$), 139.4 (PyO-**1**$'$), 141.2 (PyO-**1**$''$), 144.5 (*ipso*-Ph), 146.1 (*ipso*-Ph), 146.7 (PyO-**1**$'$), 163.9 (PyO-**1**$''$), 164.4 (PyO-**1**$''$), 166.9 (PyO-**1**$'$); elemental analysis calcd. (%) for $C_{16}H_{13}N_2O_2As\cdot0.2H_2O$ (343.81 g mol^{-1}): C: 55.89, H: 3.93, N: 8.15; found: C: 55.98, H: 4.07, N: 8.27.

Synthesis of $As(PyO)_3$ (2)

In a Schlenk flask, 2-hydroxypyridine (962 mg, 10.12 mmol) and triethylamine (1.228 g, 12.14 mmol) were dissolved in THF (20 mL). To the clear solution arsenic(III) chloride (611 mg, 3.37 mmol) was added dropwise, and the resultant white suspension was stirred at ambient temperature for 2 h. Thereafter, the white solid (Et_3NHCl) was filtered off and washed with THF (5 mL). From the combined filtrate and washings all volatiles were evaporated *in vacuo*. The residue was recrystallized in THF (2 mL). After one day storage at room temperature, colorless crystals, suitable for single-crystal X-ray diffraction, were obtained. The supernatant was decanted, the solid was washed with diethyl ether (3 mL) and dried *in vacuo*. Yield: 451 mg (1.26 mmol, 37%); ^{1}H NMR (400.1 MHz, $CDCl_3$): 6.57-

7.02 (br. m, aryl, 6H), 7.60 (br. m, aryl, 3H), 8.01 (br. m, aryl, 3H); $^{13}C\{^1H\}$ NMR (100.6 MHz, $CDCl_3$): 111.2 (br. s), 117.2 (br. s), 139.8 (br. s), 146.3 (br. s), 164.2 (br. s); elemental analysis calcd. (%) for $C_{15}H_{12}N_3O_3As$ (MW = 357.20 g mol^{-1}): C: 50.44, H: 3.39, N: 11.76; found: C: 50.11, H: 3.69, N: 11.51.

Synthesis of [PhAs(μ-PyO)$_2$)RuCl$_2$(PPh$_3$)] (3)

PhAs(PyO)$_2$ (93 mg, 273 µmol) and [RuCl$_2$(PPh$_3$)$_3$] (262 mg, 273 µmol) were dissolved in chloroform (1 mL). The dark red solution was stirred at ambient temperature for 10 min, whereupon stirring was stopped. After one day of vapor diffusion of diethyl ether into the chloroform solution at room temperature, orange crystals suitable for single-crystal X-ray diffraction were obtained. The supernatant was decanted, the solid was washed with diethyl ether (3 mL) and dried *in vacuo*. Yield: 138 mg (144 µmol, 53%).

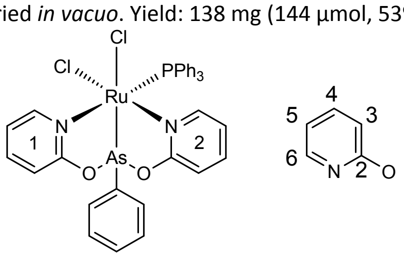

^1H NMR (500.1 MHz, $CDCl_3$): 6.19 (ddd, $^4J_{H,H}$ = 1.39 Hz, $^3J_{H,H}$ = 6.71 Hz, $^3J_{H,H}$ = 7.65 Hz, H^5 (PyO-2), 1H), 6.80 (dd, $^4J_{H,H}$ = 1.39 Hz, $^3J_{H,H}$ = 8.20 Hz, H^3 (PyO-2), 1H), 6.96-7.10 (br. m, *meta*-PPh$_3$, H^3 (PyO-1), H^5 (PyO-1), *para*-PPh$_3$, 11H), 7.23 (ddd, $^4J_{H,H}$ = 1.85 Hz, $^3J_{H,H}$ = 7.65 Hz, $^3J_{H,H}$ = 8.20 Hz, H^4 (PyO-2), 1H), 7.43 (m, *ortho*-AsPh, 2H), 7.57-7.63 (br. m, *meta*-AsPh, *para*-AsPh, H^4 (PyO-1), 4H), 7.73 (m, *ortho*-PPh$_3$, 6H), 8.71 (dd, $^4J_{H,H}$ = 1.85 Hz, $^3J_{H,H}$ = 6.71 Hz, H^6 (PyO-2), 1H), 9.74 (br. m, H^6 (PyO-1), 1H); $^{13}C\{^1H\}$ NMR (125.8 MHz, $CDCl_3$): 109.8 (s, C^3 (PyO-2)), 110.6 (s, C^3 (PyO-1)), 117.5 (s, C^5 (PyO-2)), 118.3 (s, C^5 (PyO-1)), 127.6 (d, $^3J_{C,P}$ = 9.61 Hz, *meta*-PPh$_3$), 129.1 (d, $^4J_{C,P}$ = 1.80 Hz, *para*-PPh$_3$), 124.9 (s, *meta*-AsPh), 130.2 (s, *ortho*-AsPh), 132.8 (s, *para*-AsPh), 133.6 (d, $^2J_{C,P}$ = 9.59 Hz, *ortho*-PPh$_3$), 134.7 (d, $^3J_{C,P}$ = 2.37 Hz, *ipso*-AsPh), 135.0 (d, $^1J_{C,P}$ = 45.5 Hz, *ipso*-PPh$_3$), 137.7 (s, C^4 (PyO-2)), 139.8 (s, C^4 (PyO-1)), 149.5 (s, C^6 (PyO-1)), 152.3 (s, C^6 (PyO-2)), 162.8 (s, C^2 (PyO-1)), 163.4 (s, C^2 (PyO-2)); $^{31}P\{^1H\}$ NMR (202.5 MHz, $CDCl_3$): 40.7 (s); elemental analysis calcd. (%) for $C_{34}H_{28}AsCl_2N_2O_2PRu\cdot1.4CHCl_3\cdot0.2Et_2O$ (MW = 956.42 g mol^{-1}): C: 45.46, H: 3.31, N: 2.93; found: C: 45.44, H: 3.38, N: 2.84.

Synthesis of [As(μ-PyO)$_2$)RuCl(PPh$_3$)$_2$] (5)

As(PyO)$_3$ (105 mg, 294 µmol) and [RuCl$_2$(PPh$_3$)$_3$] (282 mg, 294 µmol) were dissolved in chloroform (10 mL) and stirred at ambient temperature for 3 days. The solution was filtered through Celite, and diethyl ether (20 mL) was added to the filtrate. The mixture was stored at -24 °C for one week to afford a crystalline product. The supernatant was decanted, the yellow solid was washed with diethyl ether (8 mL) and dried *in vacuo*. Crystals suitable for single-crystal X-ray diffraction were obtained by recrystallization from chloroform. Yield: 174 mg (165 µmol, 56%);

^1H NMR (400.1 MHz, $CDCl_3$): 6.26 (dd, $^3J_{H,H}$ = 6.54 Hz, $^3J_{H,H}$ = 6.33 Hz, H^5, 2H), 6.35 (d, $^3J_{H,H}$ = 8.20 Hz, H^3, 2H), 7.01 (m, *meta*-PPh$_3$, H^4, 14H), 7.15 (t, $^3J_{H,H}$ = 7.34 Hz, *para*-PPh$_3$, 6H), 7.37 (m, *ortho*-PPh$_3$, 12H), 9.08 (d, $^3J_{H,H}$ = 6.33 Hz, H^6, 2H); $^{13}C\{^1H\}$ NMR (100.6 MHz, $CDCl_3$): 111.0 (s), 114.9 (br. s), 127.3 (dd, J = 4.50 Hz, J = 5.06 Hz), 128.7 (s), 134.2 (dd, J = 4.40 Hz, J = 5.14 Hz), 135.9 (br. m, *ipso*-PPh$_3$), 137.3 (s), 149.2 (s), 167.8 (s, C^2); $^{31}P\{^1H\}$ NMR (162.0 MHz, $CDCl_3$): 41.8 (s); elemental analysis calcd. (%) for $C_{46}H_{38}AsClN_2O_2P_2Ru\cdot1.1CHCl_3$ (MW = 1055.51 g mol^{-1}): C: 53.60, H: 3.73, N: 2.65; found: C: 53.65, H: 3.95, N: 2.66.

Synthesis of [Ph$_3$P(PyO)]Cl (6)

View Article Online
DOI: 10.1039/D0DT01808E

Triphenylphosphine (283 mg, 1.09 mmol) and 2-hydroxypyridine (100 mg, 1.05 mmol) were dissolved in acetonitrile (1 mL) and stirred for 1.5 h at 60 °C. The clear solution was evaporated to dryness, and the residue was dissolved in dichloromethane (2 mL). After one week of vapor diffusion of diethyl ether at room temperature, colorless crystals suitable for single-crystal X-ray diffraction were obtained. The supernatant was decanted, the crystalline solid was washed with diethyl ether (2 mL) and dried *in vacuo*. Yield: 302 mg (purity: ~89%, 3% impurity of Ph$_3$P=O and 8% impurity of [Ph$_3$PCH$_2$Cl]Cl; attempts of purification *via* additional recrystallization from CH_2Cl_2/Et_2O or $NCMe/Et_2O$ were not successful);

^1H NMR (500.1 MHz, $CDCl_3$): 7.25 (m, PyO, 1H), 7.62 (m, PyO, 1H), 7.75 (br. m, 6H), 7.82-7.96 (br. m, 9H), 7.99-8.07 (br. m, 2H); $^{13}C\{^1H\}$ NMR (125.8 MHz, $CDCl_3$): 112.5 (d, $^3J_{C,P}$ = 8.5 Hz, C^3, PyO), 118.0 (d, $^1J_{C,P}$ = 107.6 Hz, *ipso*-Ph), 121.7 (s, C^5, PyO), 139.2 (d, $^3J_{C,P}$ = 14.0 Hz, *meta*-Ph), 132.8 (d, $^2J_{C,P}$ = 12.2 Hz, *ortho*-Ph), 135.2 (m, *para*-Ph), 141.4 (s, C^4, PyO), 145.7 (s, C^6, PyO), 155.2 (d, $^2J_{C,P}$ = 9.2 Hz, C^2, PyO); $^{31}P\{^1H\}$ NMR (202.5 MHz, $CDCl_3$): 61.6 (s, ^{13}C satellites: $^1J_{C,P}$ = 107.6 Hz).

Synthesis of [AuCl(As(μ-PyO)$_2$)RuCl(PPh$_3$)$_2$] (7)

[RuCl(PPh$_3$)$_2$(As(PyO)$_2$)] (**5**) (40 mg, 38 µmol) and [AuCl(tht)] (14 mg, 44 µmol) were dissolved in chloroform (1 mL) and stirred at ambient temperature for 5 min. The clear solution obtained was layered with *n*-pentane (10 mL) and stored undisturbed at room temperature for crystallization. The supernatant was decanted, the solid was washed with *n*-pentane (1 mL) and dried *in vacuo*. Thereafter, the solid was dissolved in CHCl$_3$ and exposed to vapour diffusion of *n*-pentane to afford crystals suitable for single-crystal X-ray diffraction. Yield: 32 mg (27 µmol, 71%); ^1H NMR (400.1 MHz, $CDCl_3$): 6.37 (m, H^5, 2H), 6.56 (d, $^3J_{H,H}$ = 8.28 Hz, H^3, 2H), 7.11 (m, *meta*-PPh$_3$, 12H), 7.19 (ddd, $^3J_{H,H}$ = 8.28 Hz, $^3J_{H,H}$ = 7.02 Hz, $^4J_{H,H}$ = 1.86 Hz, H^4, 2H), 7.26 (t, $^3J_{H,H}$ = 7.36 Hz, *para*-PPh$_3$, 6H), 7.38 (m, *ortho*-PPh$_3$, 12H), 8.93 (d, $^3J_{H,H}$ = 6.14 Hz, H^6, 2H); $^{13}C\{^1H\}$ NMR (100.6 MHz, $CDCl_3$): 111.2 (s), 116.5 (br. s), 127.8 (dd, J = 4.62 Hz, J = 4.69 Hz), 129.6 (s), 133.9 (br. m, *ipso*-PPh$_3$), 134.5 (dd, J = 3.89 Hz, J = 4.81 Hz), 138.7 (s), 148.4 (s), 165.1 (s, C^2); $^{31}P\{^1H\}$ NMR (162.0 MHz, $CDCl_3$): 38.0 (s); elemental analysis calcd. (%) for $C_{46}H_{38}AsAuCl_2N_2O_2P_2Ru\cdot0.25CHCl_3$ (MW = 1186.46 g mol^{-1}): C: 46.82, H: 3.25, N: 2.36; found: C: 46.81, H: 3.25, N: 2.31.

Conflicts of interest

There are no conflicts to declare.

Acknowledgements

The authors thank Ute Groß for performing the elemental analyses.

Notes and references

1 a) J. S. Jones, F. P. Gabbaï, *Acc. Chem. Res.*, 2016, **49**, 857-867. b) D. You, F. P. Gabbaï, *J. Am. Chem. Soc.*, 2017, **139**, 6843–6846. c) C. R. Wade, I.-S. Ke, F. P. Gabbaï, *Angew. Chem. Int. Ed.*, 2012, **51**, 478-481. d) D. Gallego, A. Brück, E. Irran, F. Meier, M. Kaupp, M. Driess, J. F. Hartwig, *J. Am. Chem. Soc.*, 2013, **135**, 15617-15626. e) C. Jones, S. J. Black, J. W. Steed, *Organometallics*, 1998, **17**, 5924-5926. f) S.

View Article Online
DOI: 10.1039/D0DT01538E

Bestgen, N. H. Rees, J. M. Goicoechea, *Organometallics*, 2018, **37**, 4147-4155.

2 a) E. Wächtler, L. A. Oro, M. Iglesias, B. Gerke, R. Pöttgen, R. Gericke, J. Wagler, *Chem. Eur. J.,* 2017, **23**, 3447–3454. b) J. S. Jones, C. R. Wade, M. Yanga, F. P. Gabbaï, *Dalton Trans.,* 2017, **46**, 5598–5604. c) K. Toyota, Y. Wakisaka, Y. Yamamoto, K. Akiba, *Organometallics,* 2000, **19(24)**, 5122-5133.

3 J. T. Price, M. Lui, N. D. Jones, P. J. Ragogna, *Inorg. Chem.,* 2011, **50**, 12810−12817.

4 S. Burck, J. Daniels, T. Gans-Eichler, D. Gudat, K. Nättinen, M. Nieger, *Z. Anorg. Allg. Chem.,* 2005, **631**, 1403-1412.

5 C. M. Thomas, G. P. Hatzis, M. J. Pepi, *Polyhedron,* 2018, **143**, 215–222.

6 J. W. Dube, P. J. Ragogna, *Chem. Eur. J.,* 2013, **19**, 11768–11775.

7 a) V. Kremláček, J. Hyvl, W. Y. Yoshida, A. Růžička, A. L. Rheingold, J. Turek, R. P. Hughes, L. Dostál, M. F. Cain, *Organometallics,* 2018, **37**, 2481−2490. b) M. Kořenková, V. Kremláček, M. Erben, R. Jirásko, F. De Proft, J. Turek, R. Jambor, A. Růžička, I. Císařovád, L. Dostál, *Dalton Trans.,* 2018, **47**, 14503–14514. c) M. Kořenková, M. Hejda, R. Jirásko, T. Block, F. Uhlik, R. Jambor, A. Ržika, R. Pöttgen, L. Dostál, *Dalton Trans.,* 2019, **48**, 11912-11920.

8 E. A. V. Ebsworth, R. O. Gould, R. A. Mayo, M. Walkinshaw, *Dalton Trans.*, 1987, **11**, 2831-2838.

9 R. Gericke, J. Wagler, *Polyhedron,* 2017, **125**, 57–67.

10 S. S. Garje, V. K. Jain, *Main Group Met. Chem.* 1997, **20**, 755-760.

11 R. Appel, K. Warning, K.-D. Ziehn, *Liebigs Ann. Chem.,* 1975, 406-409.

12 Cambridge Structure Database, CSD v.5.40, 2019.

13 R. H. B. Mais, H. M. Powell, *J. Chem. Soc.,* 1965, 7471-7481.

14 τ_4’ was calculated as reported: A. Okuniewski, D. Rosiak, J. Chojnacki, B. Becker, *Polyhedron*, 2015, **90**, 47-57

15 R. B. Bedford, A. F. Hill, C. Jones, A. J. P. White, D. J. Williams, J. D. E. T. Wilton-Ely, *Chem. Commun.*, 1997, **2**, 179-180.

16 M. H. L. Green, *J. Organomet. Chem.,* 1995, **500**, 127-148.

17 R. F. W. Bader, Atoms in Molecules, Clarendon Press, Oxford, 1994.

18 E. Espinosa, I. Alkorta, J. Elguero, E. Molins, *J. Chem. Phys.,* 2002, **117**, 5529-5542.

19 P. Macchi, D. M. Proserpio, A. Sironi, *J. Am. Chem. Soc.,* 1998, **120**, 13429-13435.

20 A. D. Becke, K. E. Edgecombe, *J. Chem. Phys.,* 1990*,* **92**, 5397-5403.

21 A. F. Hill, G. R. Owen, A. J. P. White, D. J. Williams, *Angew. Chem., Int. Ed.*, **1999**, *38*, 2759-2761.

22 R. Gericke, J. Wagler, *Polyhedron* 2016, **120**, 134-141.

23 R. Uson, A. Laguna, M. Laguna, D. A. Briggs, H. H. Murray, J. P. Fackler, *Inorg. Synth.,* 1989, **26**, 85-91.

24 G. M. Sheldrick, *Acta Crystallogr.,* 2008, **A64**, 112-122.

25 G. M. Sheldrick, *Acta Crystallogr.,* 2015, **C71**, 3-8.

26 a) F. Neese, *WIREs Comput. Mol. Sci.,* 2012, **2**, 73-78. b) F. Neese, *WIREs Comput. Mol. Sci.,* 2018, **8**, e1327.

27 a) T. H. Dunning, Jr., *J. Chem. Phys.*, 1989, **90**, 1007. b) A. K. Wilson, D. E. Woon, K. A. Peterson, T. H. Dunning, Jr., *J. Chem. Phys.*, 1999, **110**, 7667.

28 D. Andrae, U. Häußermann, M. Dolg, H. Stoll, H. Preuss, *Theor. Chim. Acta.,* 1990, **77**, 123-141.

29 S. Grimme, J. Antony, S. Ehrlich, H. Krieg, *J. Chem. Phys.*, 2010, **132**, 154104.

30 F. Weigend, R. Ahlrichs, *Phys. Chem. Chem. Phys.,* 2005, **7**, 3297-3305.

31 E. D. Glendening, J. K. Badenhoop, A. E. Reed, J. E. Carpenter, J. A. Bohmann, C. M. Morales, C. R. Landis, F. Weinhold, *NBO 6.0* (Theoretical Chemistry Institute, University of Wisconsin, Madison, WI, 2013); http://nbo6.chem.wisc.edu/.

32 *Chemcraft ver. 1.8 (build 164),* 2016; http://www.chemcraftprog.com/.

33 T. Lu, F. Chen, *J. Comput. Chem.,* 2012, **33**, 580–592.

34 A. Michaelis, W. LaCoste, A. Michaelis, *Liebigs Ann. Chem.,* 1880, **201**, 184-261.

View Article Online
DOI: 10.1039/D0DT01538E

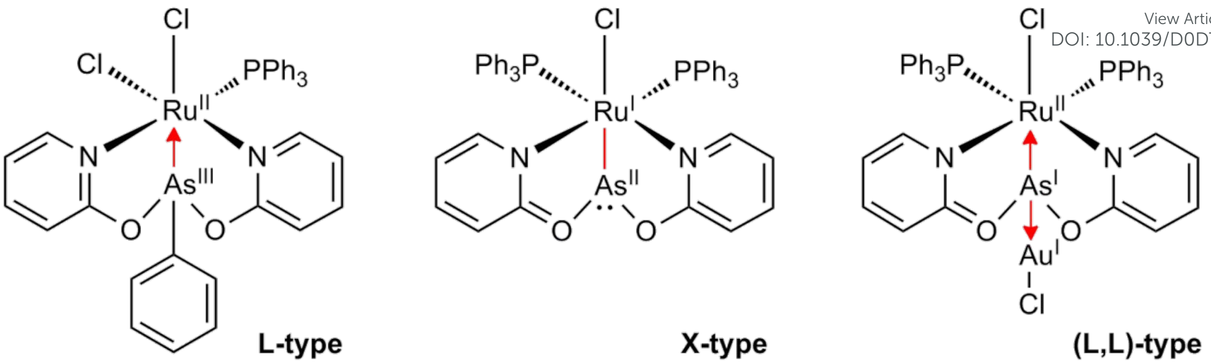

2-Pyridyloxy bridged Ru^{II}-As^{III}-complexes were shown capable of reductively eliminating an As-bound substituent with formation of Ru^{I}-As^{II} and, upon coordinating AuCl at the vacant As lone pair, Ru^{II}-As^{I} complexes.